



Trends of ozone total columns and vertical distribution from FTIR observations

C. Vigouroux et al.

Trends of ozone total columns and vertical distribution from FTIR observations at 8 NDACC stations around the globe

C. Vigouroux¹, T. Blumenstock², M. Coffey³, Q. Errera¹, O. García⁴, N. B. Jones⁵, J. W. Hannigan³, F. Hase², B. Liley⁶, E. Mahieu⁷, J. Mellqvist⁸, J. Notholt⁹, M. Palm⁹, G. Persson⁸, M. Schneider⁴, C. Servais⁷, D. Smale⁶, L. Thölix¹⁰, and M. De Mazière¹

¹Department of Atmospheric Composition, Belgian Institute for Space Aeronomy (BIRA-IASB), Brussels, Belgium

²Karlsruhe Institute of Technology (KIT), Institute for Meteorology and Climate Research (IMK-ASF), Karlsruhe, Germany

³Atmospheric Chemistry Division, National Center for Atmospheric Research (NCAR), Boulder, Colorado, USA

⁴Izaña Atmospheric Research Centre (IARC), Agencia Estatal de Meteorología (AEMET), Santa Cruz de Tenerife, Spain

⁵Centre for Atmospheric Chemistry, University of Wollongong, Wollongong, Australia

Title Page

Abstract

Introduction

Conclusions

References

Tables

Figures



Back

Close

Full Screen / Esc

Printer-friendly Version

Interactive Discussion



⁶Department of Atmosphere, National Institute of Water and Atmospheric Research Ltd (NIWA), Lauder, New Zealand

⁷Institute of Astrophysics and Geophysics, University of Liège (ULg), Liège, Belgium

⁸Department of Earth and Space Science, Chalmers University of Technology, Göteborg, Sweden

⁹Institute of Environmental Physics, University of Bremen, Bremen, Germany

¹⁰Climate Research, Finnish Meteorological Institute (FMI), Helsinki, Finland

Received: 11 July 2014 – Accepted: 29 August 2014 – Published: 25 September 2014

Correspondence to: C. Vigouroux (corinne.vigouroux@aeronomie.be)

Published by Copernicus Publications on behalf of the European Geosciences Union.

Trends of ozone total columns and vertical distribution from FTIR observations

C. Vigouroux et al.

Title Page

Abstract

Introduction

Conclusions

References

Tables

Figures



Back

Close

Full Screen / Esc

Printer-friendly Version

Interactive Discussion



Abstract

Ground-based Fourier transform infrared (FTIR) measurements of solar absorption spectra can provide ozone total columns with a precision of 2 %, but also independent partial column amounts in about four vertical layers, one in the troposphere and three in the stratosphere up to about 45 km, with a precision of 5–6 %. We use eight of the Network for the Detection of Atmospheric Composition Change (NDACC) stations having a long-term time series of FTIR ozone measurements to study the total and vertical ozone trends and variability, namely: Ny-Alesund (79° N), Thule (77° N), Kiruna (68° N), Harestua (60° N), Jungfraujoch (47° N), Izaña (28° N), Wollongong (34° S) and Lauder (45° S). The length of the FTIR time-series varies by station, but is typically from about 1995 to present. We applied to the monthly means of the ozone total and four partial columns a stepwise multiple regression model including the following proxies: solar cycle, Quasi-Biennial Oscillation (QBO), El Niño-Southern Oscillation (ENSO), Arctic and Antarctic Oscillation (AO/AAO), tropopause pressure (TP), equivalent latitude (EL), Eliassen-Palm flux (EPF), and volume of polar stratospheric clouds (VPSC).

At the Arctic stations, the trends are found mostly negative in the troposphere and lower stratosphere, very mixed in the middle stratosphere, positive in the upper stratosphere due to a large increase in the 1995–2003 period, and non-significant when considering the total columns. The trends for mid-latitude and subtropical stations are all non-significant, except at Lauder in the troposphere and upper stratosphere, and at Wollongong for the total columns and the lower and middle stratospheric columns; at Jungfraujoch, the upper stratospheric trend is close to significance ($+0.9 \pm 1.0 \%$ decade⁻¹). Therefore, some signs of the onset of ozone mid-latitude recovery are observed only in the Southern Hemisphere, while a few more years seems to be needed to observe it at the northern mid-latitude station.

ACPD

14, 24623–24666, 2014

Trends of ozone total columns and vertical distribution from FTIR observations

C. Vigouroux et al.

Title Page

Abstract

Introduction

Conclusions

References

Tables

Figures

◀

▶

◀

▶

Back

Close

Full Screen / Esc

Printer-friendly Version

Interactive Discussion



Trends of ozone total columns and vertical distribution from FTIR observations

C. Vigouroux et al.

Title Page

Abstract

Introduction

Conclusions

References

Tables

Figures

◀

▶

◀

▶

Back

Close

Full Screen / Esc

Printer-friendly Version

Interactive Discussion



simultaneously with the ozone profile, adding the microwindow 896.4–896.6 cm⁻¹ for a better H₂O determination. At Kiruna, Izaña and Jungfraujoch, the H₂O a priori profiles are only scaled in the ozone retrieval, but these a priori profiles have been preliminarily retrieved in dedicated H₂O microwindows for each spectrum (Schneider et al. (2006) for Kiruna and Izaña; Sussmann et al. (2009) for Jungfraujoch). For the very dry Jungfraujoch site, it has been found that preliminary H₂O retrievals do not improve the quality of the ozone retrievals. At Ny-Alesund and Thule, water vapor is treated as the other interfering species: only a scaling of a single a priori profile from WACCM4 is made.

In optimal estimation, the choice of the a priori covariance matrix \mathbf{S}_a is also an important parameter of the inversion process, and together with the measurement noise error covariance matrix \mathbf{S}_e , it will lead to the following averaging kernel matrix \mathbf{A} (Rodgers, 2000):

$$\mathbf{A} = (\mathbf{K}^T \mathbf{S}_e^{-1} \mathbf{K} + \mathbf{S}_a^{-1})^{-1} \mathbf{K}^T \mathbf{S}_e^{-1} \mathbf{K}, \quad (1)$$

where \mathbf{K} is the weighting function matrix that links the measurement vector \mathbf{y} to the state vector \mathbf{x} : $\mathbf{y} = \mathbf{K}\mathbf{x} + \boldsymbol{\epsilon}$, with $\boldsymbol{\epsilon}$ representing the measurement error. In our retrievals, we assume \mathbf{S}_e to be diagonal, in which case the diagonal elements are the inverse square of the signal to noise ratio (SNR). The diagonal elements of \mathbf{S}_a represent the assumed variability of the target gas volume mixing ratio (VMR) at a given altitude, and the non-diagonal elements represent the correlation between the VMR at different altitudes. This \mathbf{S}_a matrix can differ from station to station as one can see in Table 2. Except at Harestua, Kiruna and Izaña, the stations are using an a priori covariance matrix with diagonal elements constant with altitude corresponding to 10, 20 or 30 % variability, the largest variabilities taking place at the high latitude stations Ny-Alesund and Thule. At Harestua, the diagonal elements of \mathbf{S}_a correspond to 11 % in the stratosphere, decreasing down to 6 % in the troposphere and to 5 % above 35 km. Except at Ny-Alesund, the SNR value is not the real one coming from each individual spectrum, but an effective SNR, that is used as a regularization parameter. It is chosen differently from one station to another, together with the \mathbf{S}_a matrix, in order to obtain stable

retrievals with reasonable DOFS. This effective SNR is smaller than the value derived from the inherent noise in the spectra, since the residuals in a spectral fit are not only coming from pure measurement noise but also from uncertainties in the model parameters. At Kiruna and Izaña, the regularization is made using the Tikhonov L1 constraint (Tikhonov, 1963).

The observed absorption line shapes also depend on the instrument line shape (ILS) which is therefore needed in the forward models of the retrieval codes. At all stations, except Jungfraujoch and Wollongong for the Bomem spectra, the ILS has been retrieved independently from HBr or N₂O absorption measurements in a low-pressure gas cell with the LINEFIT code, as described in Hase et al. (1999). In this approach, the loss of modulation efficiency and the phase error can be described (1) by 40 parameters (20 for each) at equidistant optical path differences (OPDs); (2) or simply by two parameters assuming a linear decline of the modulation efficiency with OPD, and a constant phase error. For the Ny-Alesund, Harestua and Lauder stations, the LINEFIT results were close to, and thus have been approximated by, the ideal ILS: there is no loss of modulation efficiency vs. OPD and no phase error. At Izaña and Thule, the ILS was not ideal and the 40 parameters obtained from LINEFIT have been used to describe the ILS. At Harestua, the second option of parameters from LINEFIT was used and the phase error, which can lead to asymmetrical ILS but which was close to zero, was neglected. At Jungfraujoch, where cell measurements were not available for early years, and at Wollongong for the Bomem spectra, it also has been taken into account that the ILS may not be ideal: the ILS distortions have been approximated by an empirical apodization function that represents only symmetrical distortions (Barret et al., 2002). In the case of an ideal instrument, the apodization function would be constant and equal to 1. In case of a non-ideal ILS, the parameters of the empirical function are retrieved together with the VMR profiles, using the ideal ILS as the a priori value. A polynomial fit of order 2 and of order 4 has been used at Jungfraujoch and Wollongong, respectively. The phase error, close to zero, has been neglected.

Trends of ozone total columns and vertical distribution from FTIR observations

C. Vigouroux et al.

[Title Page](#)[Abstract](#)[Introduction](#)[Conclusions](#)[References](#)[Tables](#)[Figures](#)[Back](#)[Close](#)[Full Screen / Esc](#)[Printer-friendly Version](#)[Interactive Discussion](#)

2.3 Vertical information in FTIR retrievals

The vertical information contained in the FTIR retrievals can be characterized by the averaging kernel matrix \mathbf{A} (Eq. 1), as described in detail in Vigouroux et al. (2008). It has been shown in this previous paper that the ozone retrievals provide 4–5 DOFS, depending on the station. Therefore, in addition to total column trends, we provide ozone trends in four independent partial column layers, corresponding to the vertical information. The layer limits have been chosen such that the DOFS is at least 1.0 in each associated partial column. The adopted layers are independent according to the resolution of the averaging kernels, as can be seen in Fig. 1, where the partial column averaging kernels of the four layers in the case of Jungfraujoch are shown. Also shown is the sensitivity which is, at each altitude k , the sum of the elements of the corresponding averaging kernel $\sum_i A_{ki}$, and represents the fraction of the retrieval that comes from the measurement rather than from the a priori information. In the present work, small changes have been made in the partial column limits in comparison to Vigouroux et al. (2008): we avoid the tropopause region at each station, in order to have a better separation between the layer that we call the "tropospheric" layer, and the lower stratospheric layer. Due to the high tropopause heights at Izaña (14.9 km) and Wollongong (13.8 km), compared to mid- and high-latitude stations (from 10.1 km at Ny-Alesund to 11.8 km at Jungfraujoch), we use different partial column limits for these two stations. The upper limit of the upper layer is here 49 km, the altitude above which the sensitivity goes to zero (see Fig. 1), instead of 42 km in Vigouroux et al. (2008), the altitude above which the sensitivity is below 0.5. We still gain from 0.06 (Jungfraujoch) up to 0.23 (Lauder) DOFS in this 7 km wide range with poorer sensitivity. For Harestua, the chosen layer limits give a DOFS of only 0.9 and 0.75, in the ground 10 km and in the 29–49 km layers, respectively.

We provide in Table 3, the partial column limits for each station. The detailed error budget for ozone FTIR retrievals has been described in Vigouroux et al. (2008) and more recently in García et al. (2012) for Izaña, and we just summarize in Table 3 the

Trends of ozone total columns and vertical distribution from FTIR observations

C. Vigouroux et al.

Title Page

Abstract

Introduction

Conclusions

References

Tables

Figures



Back

Close

Full Screen / Esc

Printer-friendly Version

Interactive Discussion



total random uncertainties obtained for the present choice of layers. As obtained in the two previous papers, and not shown here, the smoothing error is the dominant random error source for the tropospheric and lower stratospheric layer, while the temperature dominates the random error budget for the middle and upper stratospheric layers, and for total columns. Also found in these two papers, and not repeated here, is the validation of the FTIR total and partial columns with correlative data (Dobson, Brewer, UV-VIs, ozonesondes, Lidar).

2.4 FTIR ozone time series

Figure 2 displays the time series of ozone total columns at each ground-based FTIR station. Because we consider only solar absorption measurements, the time series at Ny-Alesund, Thule, and Kiruna cover only the Mid-March–September, Late-February–Mid-October and Mid-January–Mid-November periods, respectively. The seasonal variation is isolated in Fig. 3 which shows the monthly mean total columns over the periods of measurements. We clearly see the well-known seasonal cycle of ozone total column having a maximum in spring at all stations, and the higher amplitude of the seasonal variation at higher latitudes (Brasseur and Solomon, 1984).

Figure 3 shows also the monthly means of the four partial columns defined in the previous section (Table 3). In the upper stratospheric layer, the ozone maximum occurs in summer (early summer at high latitudes shifting to late summer with decreasing latitude), in agreement with higher photo-chemical production of ozone during this season. In the lower stratospheric layer, the ozone maximum is in late winter/early spring at all latitudes. The situation is more contrasted for the middle stratospheric layer: still late winter/early spring for Harestua, Jungfraujoch, Lauder and Wollongong, but the latter shows a second maximum in late summer, and a small amplitude of the seasonal cycle. For the three higher latitude stations Ny-Alesund, Thule and Kiruna, the maximum is still in spring, extending to May for the two latter stations. At Izaña, the maximum is in summer in the middle stratosphere. For the tropospheric column, we observe a maximum in spring at all stations, but at Jungfraujoch it extends also in summer.

Trends of ozone total columns and vertical distribution from FTIR observations

C. Vigouroux et al.

Title Page

Abstract

Introduction

Conclusions

References

Tables

Figures



Back

Close

Full Screen / Esc

Printer-friendly Version

Interactive Discussion



3 Multiple regression model

The ozone FTIR total and partial column trends in Vigouroux et al. (2008); WMO (2010); García et al. (2012) were calculated with a bootstrap re-sampling method, applied to the daily means time series. In these studies, only the seasonal cycle and a linear trend were taken into account, the remaining natural ozone variability was then an additional noise in the ozone trend determination. To reduce the uncertainties on the trends and to better understand what drives ozone variability and trends, we use in the present study a multiple linear regression (MLR) model. To reduce the auto-correlation in the residuals, we use here the monthly means time series.

The following regression model is applied to the monthly means of ozone total and partial column time series $Y(t)$:

$$Y(t) = A_0 + A_1 \cdot \cos(2\pi t/12) + A_2 \cdot \sin(2\pi t/12) + A_3 \cdot \cos(4\pi t/12) + A_4 \cdot \sin(4\pi t/12) + A_5 \cdot t + \sum_{k=6}^n A_k \cdot X_k(t) + \epsilon, \quad (2)$$

where the A_1 to A_4 parameters describes the ozone seasonal cycle, A_5 is the annual trend, X_k are the explanatory variables (proxies time series) and A_k their respective coefficient, and ϵ represents the residuals.

To select the final regression model, we have included several proxies, which represent processes that are known to impact ozone, in a stepwise regression procedure that keeps or rejects each proxy: the initial model (seasonal cycle and trend) is fitted first. Second, iteratively, if any proxies, not already in the model, have p values less than an entrance tolerance (0.05) i.e. if it is unlikely that they would have zero coefficient if added to the model, then we add the one with the smallest p value. Otherwise, if any proxies in the model have p values greater than an exit tolerance (0.10), then we remove the one with the largest p value and we repeat the whole process until no

Trends of ozone total columns and vertical distribution from FTIR observations

C. Vigouroux et al.

Title Page

Abstract

Introduction

Conclusions

References

Tables

Figures



Back

Close

Full Screen / Esc

Printer-friendly Version

Interactive Discussion



Trends of ozone total columns and vertical distribution from FTIR observations

C. Vigouroux et al.

Title Page

Abstract

Introduction

Conclusions

References

Tables

Figures



Back

Close

Full Screen / Esc

Printer-friendly Version

Interactive Discussion



single step improves the model. Hence, the final set of parameters can vary with the station and with the partial columns concerned. In this paper, a proxy is called “non-significant” when it has not been retained by the stepwise procedure. This choice of not using a fixed model for all stations and partial columns avoids to over-fit the data, and is justified by the large latitudinal range of the stations (e.g., the VPSC or ENSO proxies will not impact the stations in the same way), and by the different processes driving ozone variability at different altitudes.

The proxies that have been tested in the stepwise regression procedure are summarized in Table 4. The two most common explanatory variables found in the literature are the solar radio flux (F10.7 index) which represents the 11 year solar cycle (following e.g. Newchurch et al., 2003; Randel and Wu, 2007), and the zonal winds measured at Singapore at 30 and 10 hPa (following e.g. Brunner et al., 2006) which represent the quasi-biennial oscillation (QBO). The proxy used for the El Niño-Southern Oscillation is the Multivariate ENSO Index (MEI), following Randel et al. (2009). Different time-lags (from 0 to 4 months) between ENSO and ozone time series have been tested. The other dynamical proxies that have been explored are the tropopause pressure at each station (following e.g. Appenzeller et al., 2000), the equivalent latitude at three altitude levels around each station (ELL, ELM, ELU), the Arctic Oscillation (AO) or the Antarctic Oscillation (AAO) indices depending on the station location (e.g. Appenzeller et al., 2000; Frossard et al., 2013), and the vertical component of the Eliassen-Palm flux (EPF) at 100 hPa averaged over 45 to 75° north and south, as a proxy for the Brewer-Dobson circulation (e.g. Brunner et al., 2006). Those proxies are connected (Appenzeller et al., 2000; Weber et al., 2011), but we let the stepwise regression model choose the most adapted proxy for each station and partial column. Concerning the equivalent latitude, we did not construct an integrated equivalent proxy valuable for the whole ozone “integrated” total column as in Wohltmann et al. (2005). Here, we simply use the equivalent latitude calculated from ERA Interim reanalysis (Dee et al., 2011) at three altitude levels corresponding approximately to the middle of our three stratospheric layers (ELL for

LowS, ELM for MidS, and ELU for UppS), namely at 370, 550, and 950 K, respectively, for all stations except Izaña and Wollongong (460, 700, and 1040 K, respectively).

Lastly, the volume of polar stratospheric clouds (VPSC) is used as a proxy for polar ozone loss (e.g. Brunner et al., 2006). The VPSC proxy has been multiplied by the effective equivalent stratospheric chlorine (EESC) time series calculated with a mean age of air of 5.5 years, in order to take into account the time for the ozone depleting substances to reach the poles (http://acdb-ext.gsfc.nasa.gov/Data_services/automailer/index.html). To account for the cumulative effect over months of the EPF and the VPSC*EESC proxies on ozone, we have followed the approach of Brunner et al. (2006) (see their Eq. 4).

For the two QBO proxies (30 and 10 hPa), if retained in the stepwise procedure, four seasonal parameters can be added to the model. The $A_k \cdot X_k(t)$ term of Eq. (2) is then replaced by:

$$(A_k + A_{k+1} \cdot \cos(2\pi t/12) + A_{k+2} \cdot \sin(2\pi t/12) + A_{k+3} \cdot \cos(4\pi t/12) + A_{k+4} \cdot \sin(4\pi t/12)) \cdot X_k(t). \quad (3)$$

Depending on the station and on the layer, none, one or both of the two proxies QBO30 and QBO10 will be retained in the model, with or without their additional seasonal parameters. We will call from here “QBO contribution”, the sum of all possible contributions of QBO30 and QBO10.

Since the time series involved in the present study start at earliest in 1995, we do not include two commonly used explanatory variables: the aerosol optical thickness needed to represent the effect on ozone of the large volcanic eruptions of El Chichón (1982) and Mount Pinatubo (1991), and the EESC proxy which can be used as direct proxy for the halogen loading of the stratosphere instead of the piecewise linear trend (PWLT) with a turnaround in 1996/1997 often used in time series starting well before this turnaround point (WMO, 2010). Our linear trend estimates are therefore better comparable to the studies which use the PWLT method. At polar stations, the turnaround is occurring a few years later, so that the use of the EESC proxy could be an

Trends of ozone total columns and vertical distribution from FTIR observations

C. Vigouroux et al.

Title Page

Abstract

Introduction

Conclusions

References

Tables

Figures



Back

Close

Full Screen / Esc

Printer-friendly Version

Interactive Discussion



alternative to the simple linear trend for these stations. However, we preferred to adopt the same approach for all the stations. Probably, when the FTIR record will be longer, one would be able to distinguish between the EESC impact on ozone and a possible additional trend due to process(es) that are not represented in the model.

To account for the auto-correlation in the residuals, a Cochrane-Orcutt transformation is applied (Cochrane and Orcutt, 1949). This gives more reliable confidence intervals for the regression parameters.

4 Results and discussion

In Fig. 4, we show the individual contribution C_{frac} of each proxy retained by the stepwise procedure to the coefficient of determination $R^2 = \sum C_{\text{frac}}$, for each station and partial column. The individual contribution C_{frac} of a proxy is the product of the standardized regression coefficient of this proxy with the correlation coefficient between the proxy and the observations (Scherrer, 1984). In Fig. 4, the seasonal parameters contribution (A_1 to A_4 in Eq. 2), which gives in most cases the very dominant part of the explained variability, is not shown for better clarity of the other proxies contribution. But we give it for completeness in Table 5, together with R^2 . In the following discussion, we will highlight some selected features which are visible in the ozone time series and which can be attributed to a specific proxy. The final MLR model is the sum of all the significant proxies, and therefore the effect of a specific proxy can be visible in the plots in some years, but masked in other years.

In Table 6, we give the annual ozone trend at each station for each layer obtained with the stepwise multiple linear regression model. The uncertainties on the trends correspond to the 95 % percent confidence interval. A trend is considered significant if it is larger than the uncertainty.

Trends of ozone total columns and vertical distribution from FTIR observations

C. Vigouroux et al.

Title Page

Abstract

Introduction

Conclusions

References

Tables

Figures



Back

Close

Full Screen / Esc

Printer-friendly Version

Interactive Discussion



4.1 High latitude stations

In addition to the three Arctic stations Ny-Alesund, Thule and Kiruna, we will consider Harestua (60° N) as a high latitude station since, in terms of trends, Harestua appears to behave similarly to the Arctic stations.

4.1.1 Tropospheric (Trop) columns

In the troposphere, the high latitude stations, except Kiruna, show negative significant ozone trends (Table 6). The spatial and temporal variability in the Arctic and the different sampling at the stations Thule/Ny-Alesund due to polar night (see Fig. 2) makes it difficult to compare the trend results. At Harestua, the negative trend is occurring in the 1995–2007 period. On the contrary, we see in Fig. 5 that at Ny-Alesund the negative trend occurs in the second part of the period (2004–2012). We see some similar features with the work of Hess and Zbinden (2013) who provide trends at 500 hPa for Northern Europe from ozonesondes: we also observe more tropospheric ozone in 1998 and 1999 and less in 2005 (their Fig. 1 compared to our middle panel of Fig. 5 where the seasonal signal is removed for emphasizing the interannual variability). We have added in Fig. 5 the VPSC signal, i.e. the VPSC proxy time series multiplied by the corresponding parameter obtained in the MLR process ($A_k \cdot X_k(t)$ in Eq. 2). We see that the discussed features (1998, 1999, 2005), but also e.g. the lower ozone values in 2011, can be explained by the VPSC proxy, therefore by the influence of lower stratospheric ozone variability on the tropospheric columns. At the three other stations, this VPSC impact was not found to be significant, and the main driver of tropospheric variability is found to be the tropopause pressure TP (Fig. 4).

4.1.2 Lower stratospheric (LowS) columns

The VPSC proxy is found significant at the four high latitude stations for the lower stratospheric columns, being the main driver of ozone variability after TP (Fig. 4). We

Trends of ozone total columns and vertical distribution from FTIR observations

C. Vigouroux et al.

Title Page

Abstract

Introduction

Conclusions

References

Tables

Figures



Back

Close

Full Screen / Esc

Printer-friendly Version

Interactive Discussion



Trends of ozone total columns and vertical distribution from FTIR observations

C. Vigouroux et al.

Title Page

Abstract

Introduction

Conclusions

References

Tables

Figures



Back

Close

Full Screen / Esc

Printer-friendly Version

Interactive Discussion



since the increase in solar activity from 1996 to its maximum in 2001–2002 is in phase with the ozone increase during the same period. The solar cycle signal at Ny-Alesund shown in Fig. 7 as an illustration turns out to be non-significant after the Cochrane-Orcutt transformation is applied, and therefore is not included in the final MLR. The solar cycle being non-significant at Kiruna, Harestua and Ny-Alesund, a trend, that would be due to it, would not taken into account in the MLR and would appear in the residual “Trend” parameter. The solar cycle might be found non-significant because the expected decrease of ozone during the declining phase of the solar cycle (2002–2009) is not observed. This could be a sign that this decrease is compensated by a positive linear trend, which could be due to the declining EESCs, but also to the increase of greenhouse gases (WMO, 2010). More years are needed to understand unequivocally the increase in 1995–2003, followed by a leveling off, and distinguish between the ozone responses due to solar cycle, EESCs and possible proxies not included in the present study.

4.1.5 Total columns

Finally, we observe that the total column ozone trends are small and non-significant at all high latitude stations, except at Ny-Alesund ($-3.0 \pm 1.5 \% \text{ decade}^{-1}$). The negative trend at Ny-Alesund occurs in the 2003–2012 period, as for the lowest altitude layers. At all stations, the dominant contributions to the total column variability are the TP, the VPSC, the EL at 950 K, and, except at Harestua, the EPF proxies. We see nicely in Table 5, how well the proxies explained the additional variability at the Arctic stations, e.g. at Ny-Alesund $R^2 = 0.95$, compared to the contribution of the seasonal cycle $C_{\text{seas}} = 0.68$.

4.2 Mid-latitude and subtropical stations

We have two mid-latitude stations in this study (Jungfraujoch, 47° N and Lauder, 45° S), and two subtropical stations (Izaña, 28° N and Wollongong, 34° S).

4.2.1 Tropospheric (Trop) columns

The tropospheric trends are non-significant at Jungfraujoch, Izaña and Wollongong, and significantly positive at Lauder. The trend at Jungfraujoch is $-2.5 \pm 2.7 \%$ decade⁻¹, but we see in Fig. 8 that the tropospheric columns are increasing up to 1999 and then show a linear decrease, in agreement with aircraft and surface alpine sites in the study of Logan et al. (2012). If we limit our time period to the 1998–2008 period as in Logan et al. (2012), we also find a significant negative trend ($-6.3 \pm 4.9 \%$ decade⁻¹). But this is largely due to the high ozone values 1998–1999, and for the period 2000–2012 we obtain still a non-significant trend of $-2.9 \pm 3.4 \%$ decade⁻¹. At Izaña, the tropospheric trends derived from ozonesondes were found non-significant in García et al. (2012), in agreement with our study, but the uncertainties were large. The situation is more mixed in the Southern Hemisphere: the tropospheric trend at Wollongong is not significant while it is significantly positive at Lauder ($+7.7 \pm 3.5 \%$ decade⁻¹). The trend at Lauder is in agreement with the study of Oltmans et al. (2013) who obtain about $+5 \%$ decade⁻¹ in the lower and middle troposphere with ozonesondes measurements at Lauder. We find a significant positive impact of the solar cycle at Lauder and it is clearly seen in Fig. 8. This is not in agreement with Chandra et al. (1999), in which the solar cycle shows a strong but negative impact on tropospheric columns for non-polluted region. At Lauder at present only a short time period (2001–2012) is available for trend studies, and we hope to have more clarification on this subject with more years of data. However, if we remove the solar cycle proxy from the MLR model, we still obtain a significant trend of $+5.0 \pm 4.4 \%$ decade⁻¹.

4.2.2 Lower stratospheric (LowS) columns

The trends in the lower stratosphere are non-significant at Jungfraujoch, Izaña and Lauder, and significantly positive at Wollongong. The dominant proxy is TP for all stations. At the Jungfraujoch station, the VPSC proxy, which in the case of Jungfraujoch corresponds to the transport of polar ozone loss to mid-latitudes, explains about 8 % of

Title Page

Abstract

Introduction

Conclusions

References

Tables

Figures



Back

Close

Full Screen / Esc

Printer-friendly Version

Interactive Discussion



4.2.5 Total columns

The total column trends are non-significant at the mid-latitude stations ($-0.4 \pm 1.2 \% \text{decade}^{-1}$ or $-1.4 \pm 3.8 \text{ DU decade}^{-1}$ at Jungfraujoch, $-0.3 \pm 1.8 \% \text{decade}^{-1}$ or $-1.1 \pm 5.9 \text{ DU decade}^{-1}$ at Lauder), non-significant at Izaña ($+0.5 \pm 1.2 \% \text{decade}^{-1}$ or $+1.4 \pm 3.6 \text{ DU decade}^{-1}$), and significantly positive at Wollongong ($+1.9 \pm 1.1 \% \text{decade}^{-1}$ or $+5.8 \pm 3.5 \text{ DU decade}^{-1}$). The total column trend at Jungfraujoch is in agreement within error bars with the result of Nair et al. (2013) at OHP when they use the PWLT method ($+5.5 \pm 3.3 \text{ DU decade}^{-1}$), but again the trend at OHP is found significantly positive. When the EESC proxy is used in their study a trend of $+4.2 \pm 0.8 \text{ DU decade}^{-1}$ is found. The same behaviour is seen more globally in a recent study using merged satellite data from 1979 to 2012 (Chehade et al., 2014): for the latitude of Jungfraujoch, the trends are about $+3\text{--}4 \text{ DU decade}^{-1}$ for the 1997–2012 period, and non-significant if the PWLT method is used, while significant when the EESC proxy is used, which decreases the uncertainty on the trends. It seems that at Jungfraujoch, our time series is still too short to observe this positive trend. At the latitude of Izaña, the merged satellite data set shows a $+3\text{--}4 \text{ DU decade}^{-1}$ for the 1997–2012 period, with the more recent SBUV/SBUV-2 MOD v8.6, non-significant using the PWLT (in agreement with our study) and significant using the EESC proxy. Since our time series start at best in 1995, the EESC proxy is not really “separable” from a linear trend study at our mid-latitude and subtropical stations. When more years of data will become available, the same sensitivity study (PWLT vs EESC) could be tested at least for polar stations where the turnaround point is expected around 2000.

It is also interesting to note that, using the PWLT method, at the latitude of Wollongong, Chehade et al. (2014) found a positive significant trend of about $+3 \text{ DU decade}^{-1}$, while at the latitude of Lauder the trend is decreased to about $+1 \text{ DU decade}^{-1}$ (non-significant) in good agreement with what FTIR observed. When they use the EESC proxy, the trend is increasing with latitude, so that at the Lauder latitude, it reaches about $4\text{--}5 \text{ DU decade}^{-1}$.

Trends of ozone total columns and vertical distribution from FTIR observations

C. Vigouroux et al.

Title Page

Abstract

Introduction

Conclusions

References

Tables

Figures



Back

Close

Full Screen / Esc

Printer-friendly Version

Interactive Discussion



Trends of ozone total columns and vertical distribution from FTIR observations

C. Vigouroux et al.

Title Page

Abstract

Introduction

Conclusions

References

Tables

Figures



Back

Close

Full Screen / Esc

Printer-friendly Version

Interactive Discussion



Our non-significant trends at Jungfraujoch, Izaña and Lauder, and positive trend at Wollongong are also in agreement with the recent study of Coldewey-Egbers et al. (2014), which provides trends using a similar period (1995–2013) of merged satellite data sets. For Wollongong, since the total column positive trend is due to the ozone trends in the lower and middle stratosphere, it cannot be attributed unambiguously to the EESCs decline.

5 Conclusions

We have exploited the time series of ozone total and partial columns (Trop, LowS, MidS, UppS) at 8 NDACC FTIR stations (Ny-Alesund, 79° N; Thule, 77° N; Kiruna, 68° N; Harestua, 60° N; Jungfraujoch, 47° N; Izaña, 28° N; Wollongong, 34° S; Lauder, 45° S) to derive vertically resolved trends, using a MLR model including the main proxies well-known for impacting the ozone variability.

After the seasonal variation, the TP proxy is the dominant driver of ozone variability at all stations, mainly for the troposphere, lower stratosphere and total columns, while the EL proxy is an important contributor to the middle and upper stratosphere, as well as to the total column variabilities. At the highest latitude stations (68 to 79° N), the EPF proxy contributes substantially to the middle stratospheric and total column variabilities. The VPSC proxy for polar ozone loss contributes to the lower stratosphere and total columns variabilities at the Arctic stations, but also at Jungfraujoch while it is non-significant at the southern hemispheric station Lauder. At the mid-latitude and subtropical stations, the QBO proxy is a substantial contributor to ozone variability, especially at the lowest latitude station, Izaña. The AO/AAO and ENSO proxies are significant only at Jungfraujoch and Izaña, respectively. At Wollongong, the 2.5 % ozone response to solar cycle in the upper layer is in agreement with previous studies, but the response in the middle stratosphere (~ 6 %) is much larger than previously reported (~ 1 %). The 11 year solar cycle effect is still subject of debate (WMO, 2010; Chiodo et al., 2014), so that an additional decade of measurements would help in fixing its real

Trends of ozone total columns and vertical distribution from FTIR observations

C. Vigouroux et al.

Title Page

Abstract

Introduction

Conclusions

References

Tables

Figures



Back

Close

Full Screen / Esc

Printer-friendly Version

Interactive Discussion



Bodeker, G. E., Hassler, B., Young, P. J., and Portmann, R. W.: A vertically resolved, global, gap-free ozone database for assessing or constraining global climate model simulations, *Earth Syst. Sci. Data*, 5, 31–43, doi:10.5194/essd-5-31-2013, 2013. 24626

Brasseur, G. and Solomon, S.: *Aeronomy of the Middle Atmosphere*, 441 pp., D. Reidel Publishing Company, Dordrecht, Holland, 1984. 24632

Brunner, D., Staehelin, J., Maeder, J. A., Wohltmann, I., and Bodeker, G. E.: Variability and trends in total and vertically resolved stratospheric ozone based on the CATO ozone data set, *Atmos. Chem. Phys.*, 6, 4985–5008, doi:10.5194/acp-6-4985-2006, 2006. 24634, 24635

Chandra, S., Ziemke, J. R., and Stewart, R. W.: An 11-year solar cycle in tropospheric ozone from TOMS measurements, *Geophys. Res. Lett.*, 26, 185–188, 1999. 24640

Chehade, W., Weber, M., and Burrows, J. P.: Total ozone trends and variability during 1979–2012 from merged data sets of various satellites, *Atmos. Chem. Phys.*, 14, 7059–7074, doi:10.5194/acp-14-7059-2014, 2014. 24626, 24643

Chiodo, G., Marsh, D. R., Garcia-Herrera, R., Calvo, N., and García, J. A.: On the detection of the solar signal in the tropical stratosphere, *Atmos. Chem. Phys.*, 14, 5251–5269, doi:10.5194/acp-14-5251-2014, 2014. 24642, 24644

Cochrane, D. and Orcutt, G. H.: Application of least squares regression to relationships containing auto-correlated error terms, *J. Am. Stat. Assoc.*, 44, 32–61, 1949. 24636

Coldewey-Egbers, M., Loyola, D. G., Braesicke, P., Dameris, M., van Roozendaal, M., Lerot, C., and Zimmer, W.: A new health check of the ozone layer at global and regional scales, *Geophys. Res. Lett.*, 41, 4363–4372, doi:10.1002/2014GL060212, 2014. 24644

Dee, D. P., Uppala, S. M., Simmons, A. J., Berrisford, P., Poli, P., Kobayashi, S., Andrae, U., Balmaseda, M. A., Balsamo, G., Bauer, P., Bechtold, P., Beljaars, A. C. M., van de Berg, L., Bidlot, J., Bormann, N., Delsol, C., Dragani, R., Fuentes, M., Geer, A. J., Haimberger, L., Healy, S. B., Hersbach, H., Hólm, E. V., Isaksen, I., Kållberg, P., Köhler, M., Matricardi, M., McNally, A. P., Monge-Sanz, B. M., Morcrette, J.-J., Park, B.-K., Peubey, C., de Rosnay, P., Tavolato, C., Thépaut, J.-N., and Vitart, F.: The ERA-Interim reanalysis: configuration and performance of the data assimilation system, *Q. J. Roy. Meteor. Soc.*, 137, 553–597, doi:10.1002/qj.828, 2011. 24634

Frossard, L., Rieder, H. E., Ribatet, M., Staehelin, J., Maeder, J. A., Di Rocco, S., Davison, A. C., and Peter, T.: On the relationship between total ozone and atmospheric dynamics and chemistry at mid-latitudes – Part 1: Statistical models and spatial fingerprints of atmospheric dy-

Trends of ozone total columns and vertical distribution from FTIR observations

C. Vigouroux et al.

[Title Page](#)[Abstract](#)[Introduction](#)[Conclusions](#)[References](#)[Tables](#)[Figures](#)[Back](#)[Close](#)[Full Screen / Esc](#)[Printer-friendly Version](#)[Interactive Discussion](#)

trend analysis of the vertical distribution of ozone, *Atmos. Chem. Phys.*, 13, 10645–10658, doi:10.5194/acp-13-10645-2013, 2013. 24626

Logan, J. A., Staehelin, J., Megretskaia, I. A., Cammas, J.-P., Thouret, V., Claude, H., De Backer, H., Steinbacher, M., Scheel, H.-E., Stübi, R., Fröhlich, M., and Derwent, R.: Changes in ozone over Europe: Analysis of ozone measurements from sondes, regular aircraft (MOZAIC) and alpine surface sites, *J. Geophys. Res.*, 117, D09301, doi:10.1029/2011JD016952, 2012. 24640

Mikuteit, S.: Trendbestimmung stratosphärischer Spurengase mit Hilfe bodengebundener FTIR-Messungen, Dissertation, Forschungszentrum Karlsruhe, FZK Report No. 7385, Germany, 2008. 24626

Nair, P. J., Godin-Beekmann, S., Kuttippurath, J., Ancellet, G., Goutail, F., Pazmiño, A., Froidevaux, L., Zawodny, J. M., Evans, R. D., Wang, H. J., Anderson, J., and Pastel, M.: Ozone trends derived from the total column and vertical profiles at a northern mid-latitude station, *Atmos. Chem. Phys.*, 13, 10373–10384, doi:10.5194/acp-13-10373-2013, 2013. 24641, 24642, 24643

Newchurch, M. J., Yang, E.-S., Cunnold, D. M., Reinsel, G. C., Zawodny, J. M., and Russell III, J. M.: Evidence for slowdown in stratospheric ozone loss: First stage of ozone recovery, *J. Geophys. Res.*, 108, 4507, doi:10.1029/2003JD003471, 2003. 24634

Oltmans, S. J., Lefohn, A. S., Shadwick, D., Harris, J. M., Scheel, H. E., Galbally, I., Tarasick, D. W., Johnson, B. J., Brunke, E.-G., Claude, H., Zeng, G., Nichol, S., Schmidlin, F., Davies, J., Cuevas, E., Redondas, A., Naoe, H., Nakano, T., Kawasato, T.: Recent tropospheric ozone changes – a pattern dominated by slow or no growth, *Atmos. Environ.*, 67, 331–351, 2013. 24640

Pougatchev, N. S., Connor, B. J., and Rinsland, C. P.: Infrared measurements of the ozone vertical distribution above Kitt Peak, *J. Geophys. Res.*, 100, 16689–16697, 1995. 24628, 24653

Randel, W. J., and Wu, F.: A stratospheric ozone profile data set for 1979–2005: Variability, trends, and comparisons with column ozone data, *J. Geophys. Res.*, 112, D06313, doi:10.1029/2006JD007339, 2007. 24634, 24641

Randel, W. J., Garcia, R. R., Calvo, N., and Marsh, D.: ENSO influence on zonal mean temperature and ozone in the tropical lower stratosphere, *Geophys. Res. Lett.*, 36, L15822, doi:10.1029/2009GL039343, 2009. 24634

Trends of ozone total columns and vertical distribution from FTIR observations

C. Vigouroux et al.

[Title Page](#)[Abstract](#)[Introduction](#)[Conclusions](#)[References](#)[Tables](#)[Figures](#)[Back](#)[Close](#)[Full Screen / Esc](#)[Printer-friendly Version](#)[Interactive Discussion](#)

Rodgers, C. D.: Inverse methods for atmospheric sounding: Theory and Practice, Series on Atmospheric, Oceanic and Planetary Physics – Vol. 2, World Scientific Publishing Co., Singapore, 2000. 24628, 24629

Rothman, L. S., Gordon, I. E., Barbe, A., Benner, D. C., Bernath, P. F., Birk, M., Boudon, V., Brown, L. R., Campargue, A., Champion, J.-P., Chance, K., Coudert, L. H., Danaj, V., Devi, V. M., Fally, S., Flaud, J.-M., Gamache, R. R., Goldman, A., Jacquemart, D., Kleiner, I., Lacome, N., Lafferty, W. J., Mandin, J.-Y., Massie, S. T., Mikhailenko, S. N., Miller, C. E., Moazzen-Ahmadi, N., Naumenko, O. V., Nikitin, A. V., Orphal, J., Perevalov, V. I., Perrin, A., Predoi-Cross, A., Rinsland, C. P., Rotger, M., Šimečková, M., Smith, M. A. H., Sung, K., Tashkun, S. A., Tennyson, J., Toth, R. A., Vandaele, A. C., and Vander Auwera, J.: The Hitran 2008 molecular spectroscopic database, *J. Quant. Spectrosc. Ra.*, 110, 533–572, 2009. 24628

Scherrer, B.: Biostatistique, Gaëtan Morin, Chicoutimi, 1984. 24636

Schneider, M., Hase, F., and Blumenstock, T.: Ground-based remote sensing of HDO/H₂O ratio profiles: introduction and validation of an innovative retrieval approach, *Atmos. Chem. Phys.*, 6, 4705–4722, doi:10.5194/acp-6-4705-2006, 2006. 24629

Sioris, C. E., McLinden, C. A., Fioletov, V. E., Adams, C., Zawodny, J. M., Bourassa, A. E., Roth, C. Z., and Degenstein, D. A.: Trend and variability in ozone in the tropical lower stratosphere over 2.5 solar cycles observed by SAGE II and OSIRIS, *Atmos. Chem. Phys.*, 14, 3479–3496, doi:10.5194/acp-14-3479-2014, 2014. 24626, 24642

Sussmann, R., Borsdorff, T., Rettinger, M., Camy-Peyret, C., Demoulin, P., Duchatelet, P., Mahieu, E., and Servais, C.: Technical Note: Harmonized retrieval of column-integrated atmospheric water vapor from the FTIR network – first examples for long-term records and station trends, *Atmos. Chem. Phys.*, 9, 8987–8999, doi:10.5194/acp-9-8987-2009, 2009. 24629

Tikhonov, A.: On the solution of incorrectly stated problems and a method of regularization, *Dokl. Acad. Nauk SSSR*, 151, 501–504, 1963. 24630

Tourpali, K., Zerefos, C. S., Balis, D. S., and Bais, A. F.: The 11-year solar cycle in stratospheric ozone: comparison between Umkehr and SBUVv8 and effects on surface erythemal irradiance, *J. Geophys. Res.*, 112, D12306, doi:10.1029/2006JD007760, 2007. 24642

Vigouroux, C., De Mazière, M., Demoulin, P., Servais, C., Hase, F., Blumenstock, T., Kramer, I., Schneider, M., Mellqvist, J., Strandberg, A., Velasco, V., Notholt, J., Sussmann, R., Stremme, W., Rockmann, A., Gardiner, T., Coleman, M., and Woods, P.: Evaluation of tropospheric and stratospheric ozone trends over Western Europe from ground-based FTIR network obser-

Trends of ozone total columns and vertical distribution from FTIR observations

C. Vigouroux et al.

Table 1. Characteristics of the FTIR stations that are contributing to the present work: location and altitude (in km a.s.l.), time-period covered by the ozone measurements used in the present trend analysis, and instrument type.

Station	Latitude	Longitude	Altitude (km)	Time-period	Instrument
Ny-Alesund	79° N	12° E	0.02	1995–2012	Bruker 120 HR
Thule	77° N	69° W	0.22	1999–2012	Bruker 120 M
Kiruna	68° N	20° E	0.42	1996–2007	Bruker 120 HR
				2007–2012	Bruker 125 HR
Harestua	60° N	11° E	0.60	1995–2009	Bruker 120 M
				2009–2012	Bruker 125 M
Jungfraujoch Izaña	47° N	8° E	3.58	1995–2012	Bruker 120 HR
	28° N	16° W	2.37	1999–2005	Bruker 120 M
Wollongong	34° S	151° E	0.03	2005–2012	Bruker 125 HR
				1996–2007	Bomem DA8
Lauder	45° S	170° E	0.37	2007–2012	Bruker 125 HR
				2001–2012	Bruker 120 HR

Title Page

Abstract

Introduction

Conclusions

References

Tables

Figures

◀

▶

◀

▶

Back

Close

Full Screen / Esc

Printer-friendly Version

Interactive Discussion



Trends of ozone total columns and vertical distribution from FTIR observations

C. Vigouroux et al.

Title Page

Abstract Introduction

Conclusions References

Tables Figures

⏪ ⏩

◀ ▶

Back Close

Full Screen / Esc

Printer-friendly Version

Interactive Discussion



Table 2. Summary of the ozone retrieval parameters. All microwindow (mw) limits are given in cm^{-1} . Ny: Ny-Alesund; Th: Thule; Ha: Harestua; Ju: Jungfraujoch.

Parameters	Ny-Alesund/Thule	Harestua/Jungfraujoch	Kiruna/Izaña	Wollongong/Lauder
Retrieval code	SFIT2 ^a v3.94	SFIT2 ^a v3.94	PROFFIT9 ^b	SFIT2 ^a v3.94
Microwindows	1000–1005 782.56–782.86 (Ny) 788.85–789.37 (Ny) 993.3–993.8 (Ny)	1000–1005	991.25–993.80 1001.47–1003.04 1005.0–1006.9 1007.347–1009.003 1011.147–1013.553	1000–1005 782.56–782.86 788.85–789.37 993.3–993.8 896.4–896.6 (H ₂ O)
H ₂ O treatment – a priori profile	One single profile (Ny) Preliminary retrievals in dedicated H ₂ O mws (Th)	One single profile (Ha) Preliminary retrievals in dedicated H ₂ O mws (Ju)	Preliminary retrievals in dedicated H ₂ O mws	One single profile
– fit in ozone mw	Scaling retrieval only	Scaling retrieval only	Scaling retrieval only	Profile retrieval
Regularization: – S _a	Diagonal: 20 % (Ny) Diagonal: 30 % (Th) No inter-layer correlation	Diagonal: 5 to 11 % (Ha) Diagonal: 10 % (Ju) No inter-layer correlation (Ha) Inter-layer correlation: gaussian decay 4 km (Ju)	Tikhonov regularization L1	Diagonal: 10 % Inter-layer correlation: exponential decay 4 km
– SNR	Real SNR (depending on each spectrum), except ^c regions at: 1000.85–1001.45 1003.16–1004.5 set to SNR = 1 (Ny) Constant = 50 (Th)	Constant = 100 (Ju) Constant = 200 (Ha)	Depending on each spectrum	Constant = 150
Instrument Line Shape	Fixed ideal (Ny) Fixed from LINEFIT (Th)	Fixed from LINEFIT (Ha) 2nd order polynomial fit of EAP (Ju)	Fixed ideal (Kiruna) Fixed from LINEFIT (Izaña)	Fixed ideal except Bomem spectra: 4th order polynomial fit of EAP

^a Pougatchev et al. (1995);

^b Hase (2000);

^c in order to mask strong H₂O absorptions.

Trends of ozone total columns and vertical distribution from FTIR observations

C. Vigouroux et al.

Table 3. Partial column (PC) limits for the 4 altitude layers containing at least one DOFS. The random uncertainties are given for each partial column. Trop: Troposphere; LowS: Lower Stratosphere; MidS: Middle Stratosphere; UppS: Upper Stratosphere; TotC: Total Columns; Gd: Ground; Err.: Total Random Uncertainties.

Layers	Stations	PC limits	Err.
Trop	Izaña/Wollongong	Gd-13/12 km	6%
	Other stations	Gd-9/10 km	5%
LowS	Izaña/Wollongong	15–23 km	5%
	Other stations	12–20 km	4%
MidS	Izaña/Wollongong	23–32 km	5%
	Other stations	20–29 km	5%
UppS	Izaña/Wollongong	31–49 km	5%
	Other stations	29–49 km	5%
TotC	Izaña/Wollongong	–	2%
	Other stations	–	2%

Title Page

Abstract

Introduction

Conclusions

References

Tables

Figures

◀

▶

◀

▶

Back

Close

Full Screen / Esc

Printer-friendly Version

Interactive Discussion



Trends of ozone total columns and vertical distribution from FTIR observations

C. Vigouroux et al.

Title Page

Abstract

Introduction

Conclusions

References

Tables

Figures

◀

▶

◀

▶

Back

Close

Full Screen / Esc

Printer-friendly Version

Interactive Discussion



Table 6. Annual trend (in % decade⁻¹) and their 95 % uncertainty ranges. Due to polar night, the measurements at Ny-Alesund, Thule and Kiruna cover only the Mid-March–September, Late-February–Mid-October, and Mid-January–Mid-November periods, respectively. All time series end in September/December 2012 for the present study. The time of start is repeated for each station. See Table 3 for the limits of the layers, different for subtropical stations and mid/high latitude stations. Trends indicated in bold are significant.

FTIR station	Trop	LowS	MidS	UppS	Total columns
Ny-Alesund 1995	-5.8 ± 3.2	-4.2 ± 3.1	-5.5 ± 3.8	+6.7 ± 5.3	-3.0 ± 1.5
Thule 1999 (October)	-5.3 ± 4.4	-0.4 ± 6.3	+0.2 ± 4.4	-2.3 ± 6.5	-2.1 ± 2.6
Kiruna 1996	-0.9 ± 2.5	-3.9 ± 2.6	+0.4 ± 2.6	+7.4 ± 3.4	-0.3 ± 1.6
Harestua 1995	-3.1 ± 2.0	-5.3 ± 4.6	+4.8 ± 4.3	+7.8 ± 5.5	+1.0 ± 2.2
Jungfrauoch 1995	-2.5 ± 2.7	-0.5 ± 3.3	-0.6 ± 1.2	+0.9 ± 1.0	-0.4 ± 1.2
Izaña 1999	+0.7 ± 2.8	-1.7 ± 2.2	-0.1 ± 2.0	+1.6 ± 2.6	+0.5 ± 1.2
Wollongong 1996	-2.2 ± 2.8	+3.1 ± 2.7	+4.0 ± 2.0	+0.2 ± 1.6	+1.9 ± 1.1
Lauder 2001	+7.7 ± 3.5	-3.8 ± 4.1	-0.2 ± 3.5	+2.8 ± 2.4	-0.3 ± 1.8

Trends of ozone total columns and vertical distribution from FTIR observations

C. Vigouroux et al.

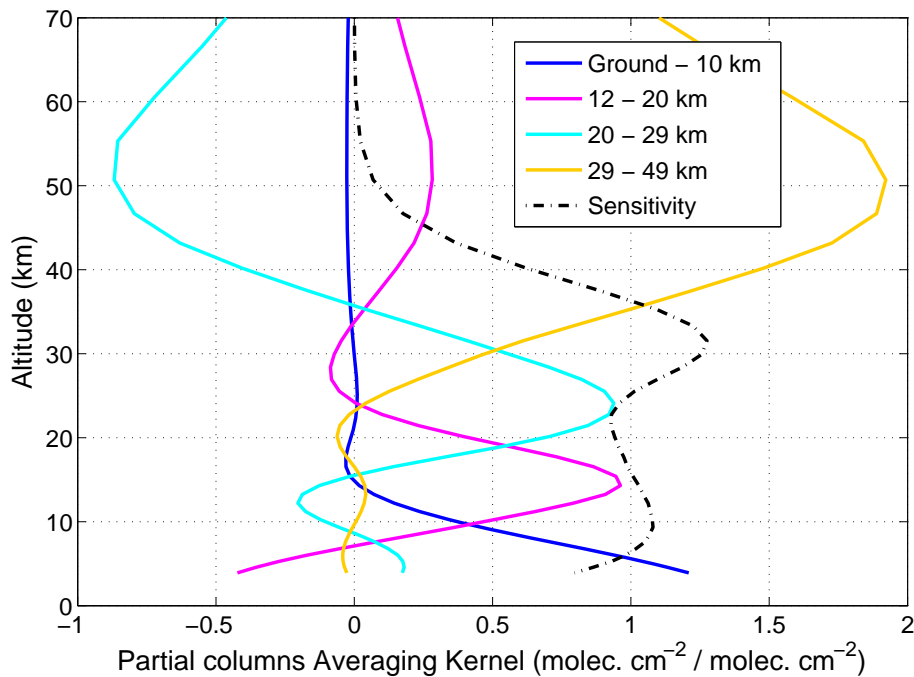


Figure 1. Partial column averaging kernels ($\text{molec. cm}^{-2} (\text{molec. cm}^{-2})^{-1}$) for ozone retrievals at Jungfraujoch station.

Title Page

Abstract

Introduction

Conclusions

References

Tables

Figures

◀

▶

◀

▶

Back

Close

Full Screen / Esc

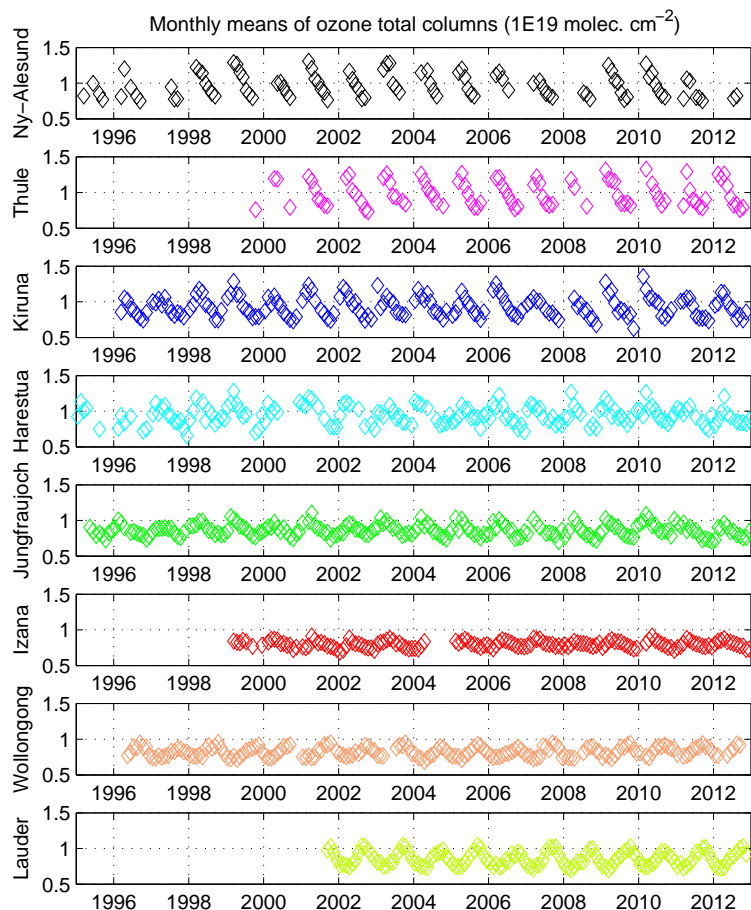
Printer-friendly Version

Interactive Discussion



Trends of ozone total columns and vertical distribution from FTIR observations

C. Vigouroux et al.

**Figure 2.** Time series of monthly means of ozone total columns at each station.[Title Page](#)[Abstract](#)[Introduction](#)[Conclusions](#)[References](#)[Tables](#)[Figures](#)[◀](#)[▶](#)[◀](#)[▶](#)[Back](#)[Close](#)[Full Screen / Esc](#)[Printer-friendly Version](#)[Interactive Discussion](#)

Trends of ozone total columns and vertical distribution from FTIR observations

C. Vigouroux et al.

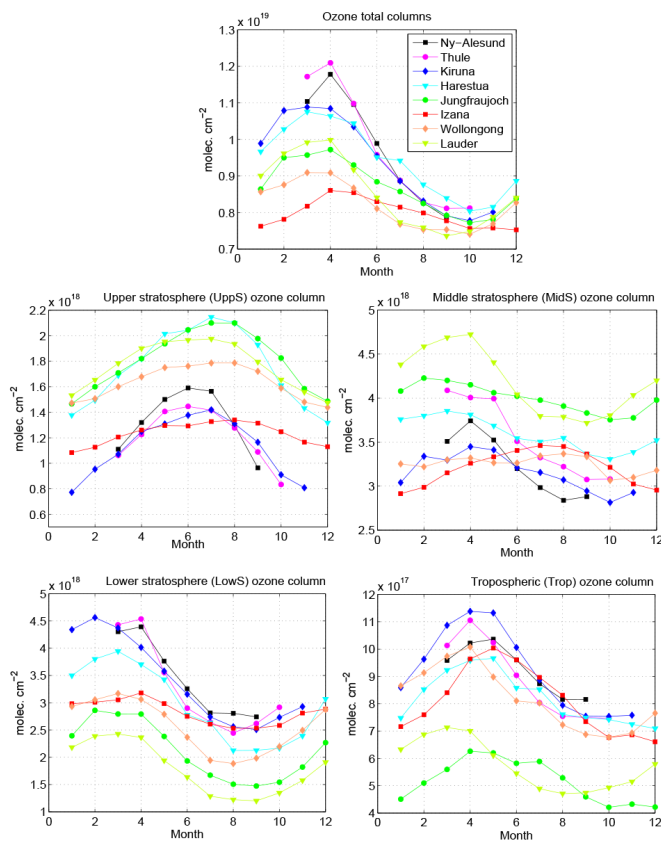


Figure 3. Monthly means of ozone total and partial columns for the whole periods of measurements. See Table 3 for the limits of the partial columns at each station. The seasonal cycle for Southern Hemisphere stations, Wollongong and Lauder, has been shifted by 6 months for better comparison.

Trends of ozone total columns and vertical distribution from FTIR observations

C. Vigouroux et al.

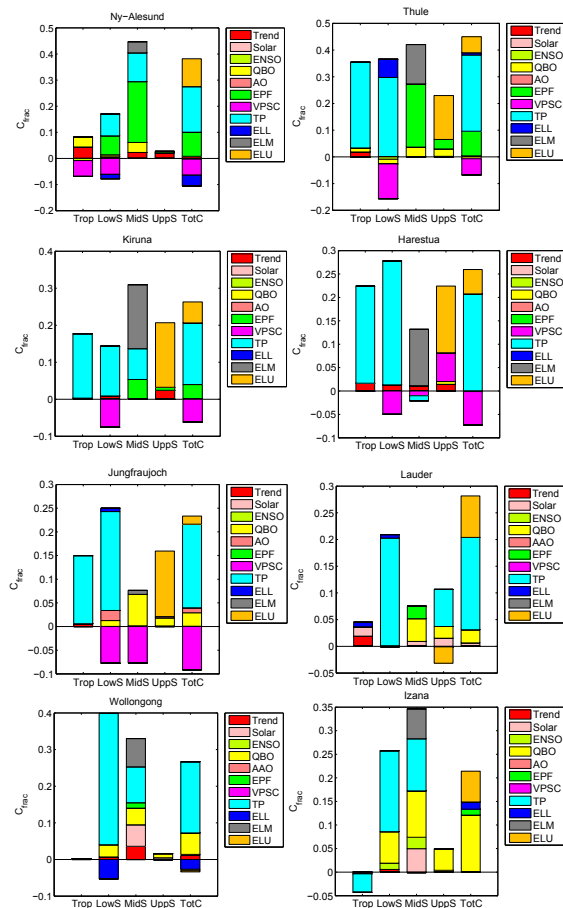


Figure 4. Individual contributions C_{fract} of the proxies to the coefficient of determination R^2 . R^2 and the dominant contribution of the seasonal cycle C_{seas} are given in Table 5.

Title Page

Abstract	Introduction
Conclusions	References
Tables	Figures

◀
▶

◀
▶

Back Close

Full Screen / Esc

Printer-friendly Version

Interactive Discussion



Trends of ozone total columns and vertical distribution from FTIR observations

C. Vigouroux et al.

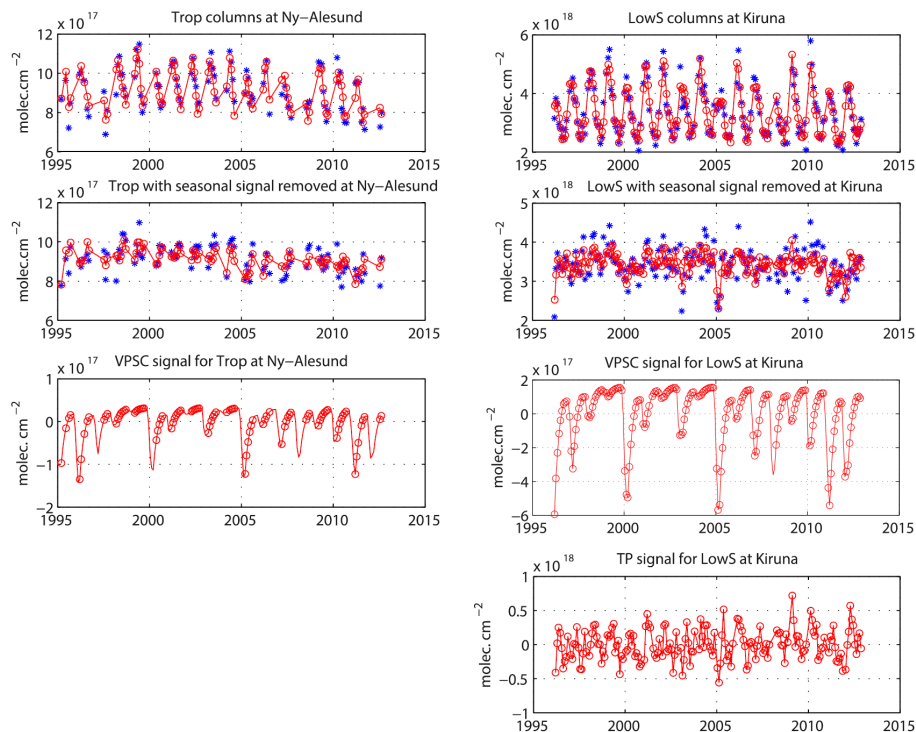


Figure 5. Top panels: monthly means of the tropospheric columns (Trop) at Ny-Alesund (left) and of the lower stratospheric columns (LowS) at Kiruna (right) (blue: FTIR, red: MLR model). Middle panels: same but with the seasonal signal removed. Bottom panels: the VPSC signal obtained in each case from the MLR model, for each month of the period (red line), and at each FTIR observed month (red circle). The tropopause pressure (TP) signal obtained for the LowS at Kiruna is also shown.

Trends of ozone total columns and vertical distribution from FTIR observations

C. Vigouroux et al.

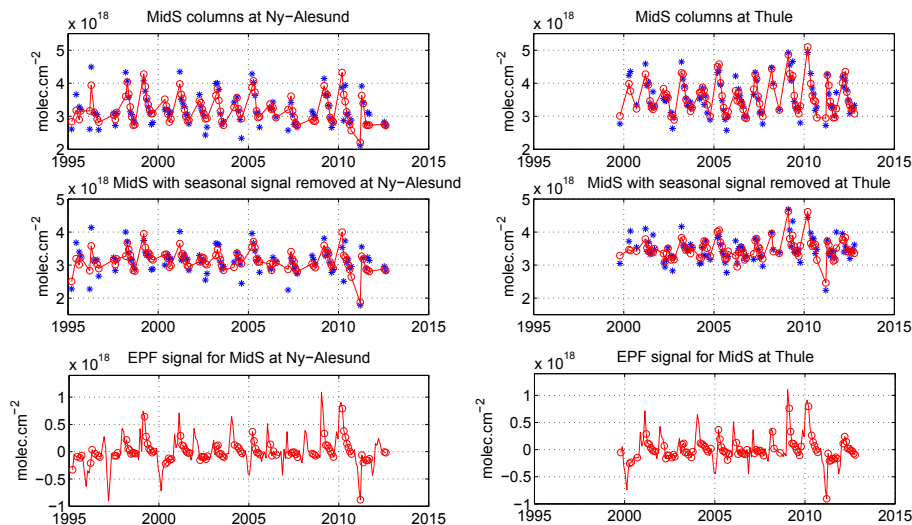


Figure 6. Top panels: monthly means of the middle stratospheric columns (MidS) at Ny-Alesund (left) and Thule (right) (blue: FTIR, red: MLR model). Middle panels: same but with the seasonal signal removed. Bottom panels: the EPF signal obtained in each case from the MLR model, for each month of the period (red line), and at each FTIR observed month (red circle).

[Title Page](#)
[Abstract](#)
[Introduction](#)
[Conclusions](#)
[References](#)
[Tables](#)
[Figures](#)

[Back](#)
[Close](#)
[Full Screen / Esc](#)
[Printer-friendly Version](#)
[Interactive Discussion](#)


Trends of ozone total columns and vertical distribution from FTIR observations

C. Vigouroux et al.

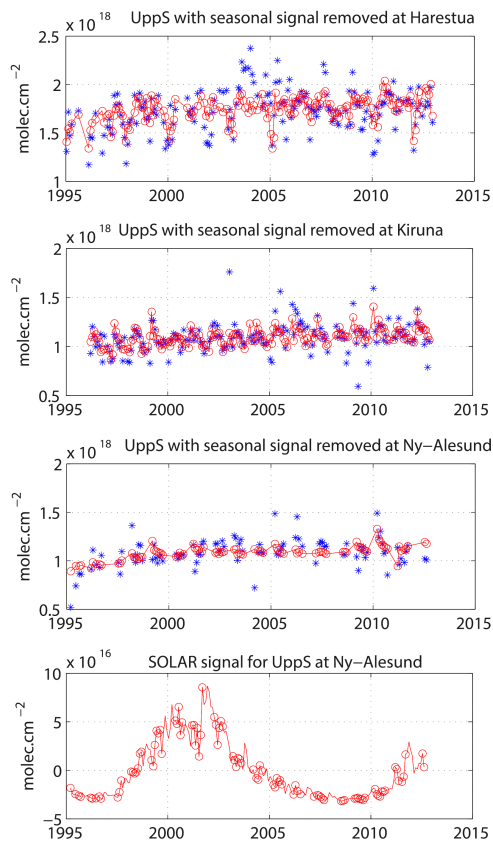


Figure 7. Monthly means of the upper stratospheric columns (UppS) with the seasonal cycle removed at, from top to bottom: Harestua, Kiruna and Ny-Alesund (blue: FTIR, red: MLR model). Bottom panel: the solar cycle signal obtained at Ny-Alesund from the MLR model, before the Cochrane-Orcutt transformation.

[Title Page](#)[Abstract](#)[Introduction](#)[Conclusions](#)[References](#)[Tables](#)[Figures](#)[◀](#)[▶](#)[◀](#)[▶](#)[Back](#)[Close](#)[Full Screen / Esc](#)[Printer-friendly Version](#)[Interactive Discussion](#)

Trends of ozone total columns and vertical distribution from FTIR observations

C. Vigouroux et al.

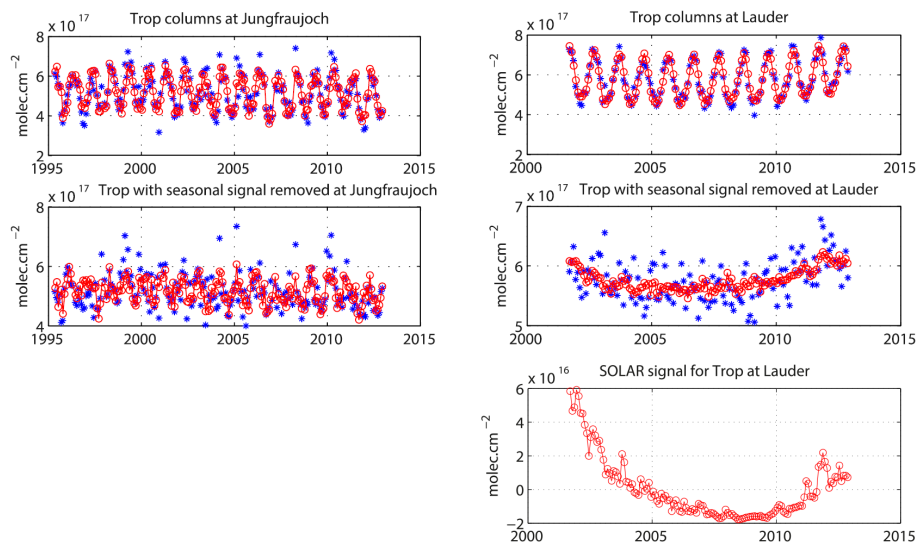


Figure 8. Top panels: monthly means of the tropospheric columns (Trop) at Jungfraujoch (left) and Lauder (right) (blue: FTIR, red: MLR model). Middle panels: same but with the seasonal signal removed. Bottom panel: the solar cycle signal obtained at Lauder from the MLR model.

Trends of ozone total columns and vertical distribution from FTIR observations

C. Vigouroux et al.

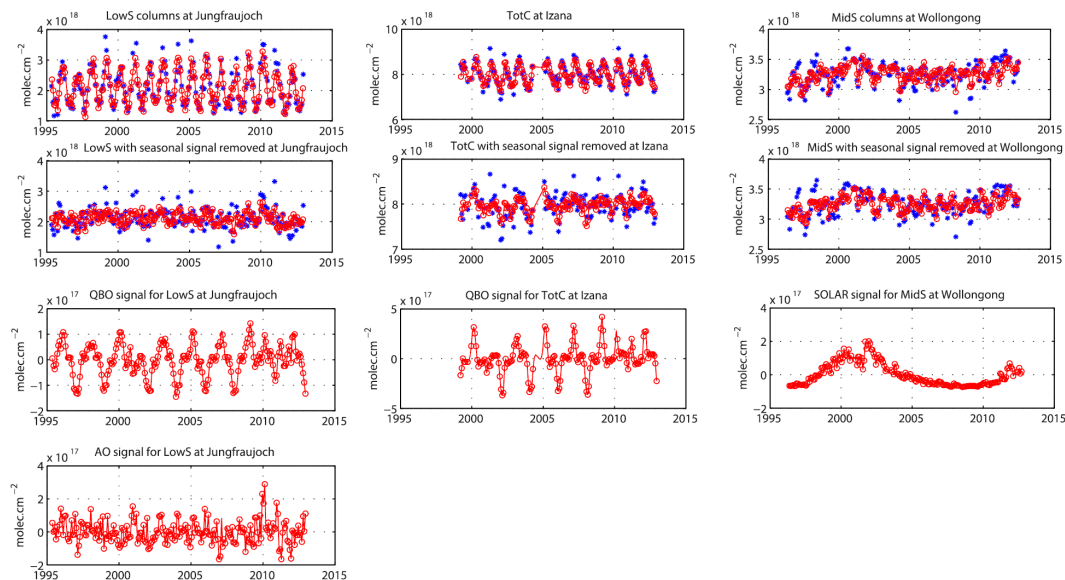


Figure 9. Top panels: monthly means of the lower stratospheric columns (LowS) at Jungfraujoch (left), total columns (TotC) at Izaña (middle), and middle stratospheric columns (MidS) at Wollongong (right). (blue: FTIR, red: MLR model). Middle panels: same but with the seasonal signal removed. Bottom panels: QBO and AO signals obtained from the MLR model at Jungfraujoch (left), QBO signal at Izaña (middle), and SOLAR signal at Wollongong (right).

[Title Page](#)
[Abstract](#)
[Introduction](#)
[Conclusions](#)
[References](#)
[Tables](#)
[Figures](#)
[Back](#)
[Close](#)
[Full Screen / Esc](#)
[Printer-friendly Version](#)
[Interactive Discussion](#)